Manuscript prepared for Hydrol. Earth Syst. Sci. Discuss.
with version 2.0 of the LaTeX class copernicus_discussions.cls.
Date: 31 March 2011

Effect of radar rainfall time resolution on the predictive capability of a distributed hydrologic model

A. Atencia[1,2], **L. Mediero**[3], **M. C. Llasat**[2], **and L. Garrote**[3]

[1]Meteorological Service of Catalonia, Barcelona, Spain
[2]Department of Astronomy and Meteorology, Faculty of Physics, University of Barcelona, Barcelona, Spain
[3]Department of Hydraulic and Energy Engineering, Technical University of Madrid, Madrid, Spain

Correspondence to: A. Atencia (aatencia@meteo.cat)

Abstract

The performance of a hydrologic model depends on the rainfall resolution, both spatially and temporally. As the spatial distribution of rainfall exerts a great influence on both runoff volumes and peak flows, the use of a distributed hydrologic model can improve the results in the case of convective rainfall in a basin where the storm area is smaller than the basin area. The aim of this study was to perform a sensitivity analysis of the rainfall time resolution on the results of a distributed hydrologic model in a flash-flood-prone basin. Because this kind of flood is produced by heavy rainfall events with a large convective component, for which radar estimation exhibits poor accuracy, a second objective was the proposal of a methodology that improves the radar rainfall estimation at a higher spatial and temporal resolution. Composite radar data from a network of three C-band radars with 6-minute temporal and $2 \times 2\,\mathrm{km}^2$ spatial resolution were used to feed the RIBS distributed hydrological model. A modification of the Window Probability Matching Method (gauge-adjustment method) was applied to four cases of heavy rainfall to improve the observed rainfall sub-estimation by computing new Z/R relationships for both convective and stratiform reflectivities. An advection correction based on the cross-correlation between two consecutive images was introduced to obtain several time resolutions from 1 min to 30 min. The RIBS hydrologic model was calibrated with a probabilistic approach based on a multiobjective methodology for each time resolution. A sensitivity analysis of rainfall time resolution was conducted to find the resolution that best represents the hydrological basin behaviour.

1 Introduction

Accurate flash flood hydrological modelling requires both a suitable hydrologic model and appropriate spatial and temporal resolutions for rainfall estimation. The spatial variability of rainfall exerts great influence on basin processes (Winchell et al., 1998), especially in the case of convective precipitation events, as the storm area is usually smaller than the basin area (Bell and Moore, 2000). The spatial distribution of rainfall influences runoff volumes, peak flows

and the lag time of hydrographs (Krajewski et al., 1991; Arnaud et al., 2002). Therefore, a distributed model can improve the simulation of flash floods events from a lumped model, as the former takes into account the spatial variability of rainfall. Furthermore, a more recent study has shown that distributed model simulations are statistically distinguishable from the lumped model simulations for basin areas around 1000 km^2 (Carpenter and Georgakakos, 2006).

The success of hydrological models is usually constrained by the rainfall data they use. Such input data could be provided by rain gauge networks and deterministic or even probabilistic meteorological models. These data sources usually present serious disadvantages for mid-size and small basins with irregular spatial rainfall distributions. Surface rain gauge networks with the appropriate resolution as raw input for accurate hydrological modelling are rare, and it is not so easy to implement a meteorological model with a sufficiently high grid resolution due to data and computational requirements. Meteorological radar can solve this problem thanks to indirect rainfall estimations at higher spatial and temporal resolutions.

However, this indirect estimation presents different sources of errors, from ground clutter or beam overshooting (Sánchez-Diezma et al., 2001) to radar calibration or attenuation (Delrieu et al., 2000). These errors could be reduced by removing static radar echoes, periodic maintenance or selecting the highest reflectivity value from each of the radars of which the network is composed. Once these errors have been partially removed and the reflectivity has been interpolated into different levels called the Constant Altitude Plan Position Indicator (CAPPI), the rainfall intensity can be obtained by applying a Z/R relationship to the lowest CAPPI reflectivity value. The literature shows many Z/R relations, from the classical Marshall and Palmer (1948) to more recent ones for different climate types, rain regimes and climatic seasons (Lee and Zawadzki, 2005; Sánchez-Diezma et al., 2000; Steiner et al., 1995; Haddad et al., 1997, to name just a few contributions).

The choice of one or another Z/R relation could alter the rainfall intensity obtained. Several methods have been developed in recent years over the Mediterranean area to obtain a suitable QPE, although they are strongly dependent on case studies. Apart from Z/R relations, there are other methods for obtaining a suitable rainfall field. Some of the latest methods are related to the direct correction of rainfall maps using multi-linear regression (Morin and Gabella, 2007),

merging rain gauge and radar data by means of non-parametric spatial models (Velasco-Forero et al., 2004) or studying the Vertical Profile of Reflectivity (Franco et al., 2008). Matching the unconditional probabilities of rainfall intensity obtained from rain gauges and reflectivity (Rosenfeld et al., 1994) is another approach to this problem. This method, which is known as Window Probabilistic Matching Method (WPMM), will be applied in this paper.

Another problem is that the rainfall intensity, especially the convective one, is a continuously varying field due to flux advections or mountain enhancement. It has been shown that sampling errors can be large, but they are easily avoidable given the computing power available today (Fabry et al., 1994). According to this article, the best methodology to avoid this sampling error is an advection correction scheme based on a cross-correlation technique (Rinehart and Garvey, 1978) and temporal linear intensity variation. Moreover, this study shows that the intensity variation between images is based on the temporal interpolation proposed by Anagnostou and Krajewski (1999) but taking into account that the shape morphology transformation is conducted by means of temporal weights based on a more complex shape transformation (Turk and O'Brien, 2005).

The Real-time Interactive Basin Simulator (RIBS) is a topography-based, rainfall-runoff model that can be used for real-time flood forecasting in mid-size and large basins (Garrote and Bras, 1995a). Once the rainfall is well estimated and a suitable hydrological model is applied, the key factor is the calibration of the hydrological model. Non-linear features of distributed models could amplify the intrinsic rainfall errors (Smith et al., 2004). For this reason, distributed models are optimised for real-time flood simulations, and some physical processes are parameterised. The parameterisation of these physical processes requires the calibration of some variables. In an early work about parameterisation in distributed models (Refsgaard, 1997), it was demonstrated that the lack of field data means that the calibration parameters lose some of their physical basis. According to their non-physical meaning and taking into account the inherent variability of these parameters, it has been shown by Madsen (2003) that the best way to estimate the value of these parameters is based on multiple objective functions. In previous works (Mediero et al., 2007; Garrote et al., 2007; Mediero et al., 2011), a probabilistic calibration was proposed for distributed models to be used in flood forecasting. This calibration

technique, and the consequent output discharge obtained, has a dependence on spatial and temporal rainfall scales. The optimal horizontal resolution is determined by low-scale hydrological processes, such as hill-slope processes (Robinson et al., 1996) or catchment processes (Yang et al., 2000). Because of this, it could be concluded that the best horizontal rainfall resolution is the highest one. Temporal variability exhibits a different hydrological behaviour. Some authors have determined a characteristic time scale for hydrological response (Morin et al., 2001), from minutes to hours. This fact could be related to concentration time or flow propagation processes, so discovering the optimal rainfall time resolution for a probabilistically calibrated distributed model would be extremely useful to determine the best input rainfall time step.

The goal of this study was to perform a sensitivity analysis of the rainfall time resolution on the results of the RIBS hydrologic distributed model to implement a real-time flood forecasting scheme in the Bess flash-flood-prone basin. For this purpose, the WPMM methodology is applied to obtain the best Z/R relation. The advection correction scheme allows for the downscaling of radar imagery from several minutes to one minute and is simultaneously used to improve the rainfall estimation. The RIBS model is calibrated for the Besòs River Basin for different time resolutions, and a sensitivity analysis of the rainfall time resolution is performed.

2 RIBS hydrologic model

The Real-time Interactive Basin Simulator (RIBS) is a topography-based, rainfall-runoff model that can be used for real-time flood forecasting in midsize and large basins (Garrote and Bras, 1995a,b). The use of this model is especially attractive when spatially distributed rainfall is available, e.g., rainfall observed from a meteorological radar station or forecasts of spatially distributed rainfall.

The RIBS model is largely based on the detailed topographical information provided by digital elevation models (DEM). Basin representation adopts the rectangular grid of the DEM, and other soil properties, input data and state variables are also represented as data layers using the same scheme. The basic objective is to map the topographically driven evolution of saturated areas as the storm progresses. Two modes of runoff generation are simulated: infiltration excess runoff and saturation excess surface runoff. RIBS applies a kinematic model of infiltration to

evaluate local runoff generation in grid elements and also accounts for lateral moisture flow between elements in a simplified manner.

Saturated hydraulic conductivity is assumed to increase with depth, following the relation

$$K_{S_y}(y) = K_{0n} \cdot e^{-fy} \tag{1}$$

where K_{0n} [mm h^{-1}] is the saturated hydraulic conductivity at the surface in the direction normal to the surface, y [mm] is the depth and f [mm^{-1}] is a parameter that controls the reduction of saturated hydraulic conductivity with the depth. There is an anisotropy between the hydraulic conductivity in the directions that are normal and parallel to the soil surface described by the anisotropy ratio α:

$$\alpha = \frac{K_{0p}}{K_{0n}} \tag{2}$$

where K_{0p} [mm h^{-1}] is the saturated hydraulic conductivity at the surface in the direction parallel to the surface.

Flow propagation to the basin outlet is computed through a distributed convolution using a Dirac delta function as an instantaneous response function for each element, with a delay equal to the time of travel from the location of the element to the basin outlet.

To obtain the travel time to the basin outlet, the speeds for the hillslope (v_h) and stream (v_s) must be defined. Stream velocity is assumed to depend on the discharge at the basin outlet:

$$v_s(t) = C_v[Q(t)]^r \tag{3}$$

where $v_s(t)$ [m/s] is the stream velocity at time t, *Q(t)* is the discharge [m^3/s] at the basin outlet and time t and C_v and r are parameters.

The hillslope velocity is related to the stream velocity through the parameter K_v:

$$K_v = \frac{v_s(t)}{v_h(t)} \tag{4}$$

where $v_h(t)$ [m/s] is the hillslope velocity at time t and K_v is a parameter.

The model captures the main features of runoff generation processes in watersheds while maintaining computational efficiency for real-time use.

3 Case studies and data

Catalonia is a region situated in the northeast corner of the Iberian Peninsula. Due to its proximity to the warm Mediterranean sea and its complex orography, with several mountain ranges parallel to the seashore line (Fig. 1), the presence of atmospheric instability usually produces intense precipitation events during the summer and autumn seasons (Llasat et al., 2003). These heavy rainfall phenomena caused 217 floods over Catalonia from 1901 to 2000, of which more than 59% were flash flood events (Barnolas and Llasat, 2007). The hydrologic timescale of most watersheds is on the order of a few hours, and flash floods develop rapidly during the early autumn season and suddenly inundate town streams, putting citizens at high risk.

One of the most prone basins in Catalonia is the Besòs Basin (Fig. 1). The Besòs catchment (1020 km^2) is located to the north of Barcelona over one of the most densely populated watersheds in Catalonia, with more than two million people living in the area. It is a typical example of the complex Mediterranean catchments, possessing great heterogeneity, from mountains over 1000 m high to rural plains that have been undergoing a continuous urbanisation process over recent decades. After two catastrophic floods in Spain in 1982, considerable investment was devoted to monitoring the catchments for hydrological purposes. It is now instrumented by several telemetered rain and streamflow gauges (see Fig. 2) from SAIH (Automatic System of Hydrological Information) of the Catalan Water Agency (ACA) to a river park built in the river mouth to mitigate flood impacts.

The present work analyses four flash flood events with great social impact (Llasat et al., 2008) that were studied within the framework of the FLASH project. The most relevant rainfall amounts for these cases are detailed in Table 1. For each case, rainfall amounts over the Besòs Basin higher than 46 mm were recorded. The peak 5-minute intensities during these events were from 80 mm/h to 135 mm/h.

The available ground rainfall data come from two different networks. The SAIH rain gauge network of the Catalan Agency of Water (ACA, hereinafter) is composed of 126 tipping-bucket automatic rain gauges covering an area of about 16 000 km^2 called the Internal Basins of Catalonia (IBS) (Fig. 1). The precipitation is accumulated and recorded every 5 min. In this study, all of the 5-min series were submitted to data quality control (Ceperuelo and Llasat, 2004).

The second network, called XEMA (Automatic Weather Station Network) is supported by the Catalan Meteorological Service (SMC) and is composed of 158 rain gauges and covers all of Catalonia (around 32 114 km^2). This network records the precipitation in two different temporal intervals. There are 47 stations that accumulate the precipitation every 30 min, while the remaining 111 stations have one-hour temporal resolution.

The merging of both networks produces a loss in temporal resolution (1 hour) and a density of about 1 rain gauge per 100 km^2, which is insufficient to reproduce the spatial pattern of most storms (Corral et al., 2001). Consequently, radar information is essential to simulate flash floods. In this work, the ACA network was used to compute the new Z/R relationship, whereas the SMC network was used to verify the results.

The radar rainfall estimation was implemented using data from the Catalan Meteorological Service (SMC) radar network, which covers an area of 53 000 km^2 over Catalonia and its surroundings. This network is made up of three C-band Doppler radars; a new radar was inaugurated in September 2008 but was not used in this study. The most important characteristics of the composed CAPPI imagery are the spatial resolution ($2 \times 2\,km^2$), time resolution (6 min) and vertical resolution (1 km) from 1 km to 10 km of altitude (10 levels). The CAPPI are calculated by means of the IRIS program, which is based on the linear interpolation of the range to the selected heights in spherical coordinates, with a correction for the earths curvature to preserve data quality. The radar imagery was corrected using SMC by first passing a filter to remove ground clutter (Bech et al., 2003). A second filter was applied to remove the interference between radars (no data in radar location) and another still target, such as a wind power plant.

The hydrological data were taken from a stream-flow gauge network composed of 100 stations from which six are located in the Besòs Basin (Fig. 2). The catchment is well covered by the SMC radar (overlap of three radar domains). Other necessary data for the hydrological model include the digital elevation model and soil type, which have been provided by the Cartographic Institute of Catalonia (ICC) with a 200 m $\times$ 200 m resolution. The function of this geomorphologic data will be explained in the Methodology section.

4 Methodology

The proposed methodology was used to perform a sensitivity analysis of the rainfall time resolution on the results of a hydrologic model in a flash-flood-prone basin. As a distributed hydrologic model is selected to better represent the spatial variations of rainfall in time, spatially distributed rainfall maps for different time resolutions were obtained from the 6-minutal radar rainfall observed. The calibrated hydrologic model was run taking these estimated rainfall maps as input data to determine the time resolution that best represents the hydrological basin behaviour.

The methodology is divided into two parts. The first part describes the estimation of the radar rainfall maps for different time resolutions. The second part describes the probabilistic calibration of the RIBS hydrologic model and the sensitivity analysis of the rainfall time resolution for the results of the calibrated RIBS model.

4.1 Radar rainfall Estimation

4.1.1 Method to calculate Z/R relation

In a previous work (Atencia et al., 2008), a large number of Z/R relations were tested for four selected heavy rainfall events. This study showed that radar-based rainfall data underestimated what rain gauges registered by approximately 18% (56 mm), and consequently, the results were not suitable for hydrological purposes.

To address the issue of QPE, a Z/R relation was obtained by applying the WPMM. This method (Rosenfeld et al., 1994) is based on matching the unconditional probabilities of rainfall and reflectivity. Obviously, point measures from radar and rain gauges are plagued by timing and spatial errors. Many of the timing and geometrical errors can be eliminated by applying the probability matching method using synchronous time series (Rosenfeld et al., 1993). This is achieved by matching rain-gauge intensities to radar reflectivities taken only from small windows centred over the gauges in time and space. Zawadzki (1975) has shown that both the window area (A) and the spread of the rain-gauge measurement in time (T) are related as fol-

lows:

$$T = \frac{1}{3} \cdot \frac{A^{\frac{1}{2}}}{V} \tag{5}$$

where V [km/h] represents the horizontal velocity of the rainfall/storm-cell system. Atlas et al. (1990) and Rigo (2004) reported a climatic horizontal velocity of convective rainfall area of about 20 km/h. Thus, the use of 3×3 pixel windows involves the use of a rain gauge time concentration of 6 min. In this study, the rain gauge had a time resolution of 5 min, but a temporal window of 30 min is used, which is a time interval that is greater than the optimal value. This fact ensures an optimal correlation between both radar and rain gauge rainfall measurements (Rosenfeld et al., 1994). Moreover, the radar time resolution (6 min) is optimum for the selected window. In this case, radar windows could be constructed. Each radar window is considered a single measurement that can be selected at random, independent of other windows. The process used to construct an all-windows dataset is divided into three steps:

- First, the radar window (3×3 pixels) around the rain gauge is selected (Fig. 3).
- Second, the independent window for each rain gauge for every period of 30 min is composed of six 5-minute intensities from the ACA rain gauge (Fig.4a)
- Third, each reflectivity's independent window for every period of 30 min is taken from every pixel (45 in total) coming from five radar windows of each 6-minute radar image (Fig. 4b)

Once the overall dataset of the independent windows has been built, the Z/R relation can be calculated from a random sub-sample of that data. To reproduce the original method (Rosenfeld et al., 1994), which was used to compute the Z/R relationship by comparing quantiles, a non-parametric technique should be used. To avoid problems of tail stability found in the empirical probability distribution function (Kaplan and Meier, 1958), a technique based on a kernel smoothing density function (Parzen, 1962) is applied. To test another smoothed relation, different parametric PDFs were fitted for both rainfall and reflectivity distributions. The ones

that maximise the likelihood were exponential functions for rain gauges, whereas the reflectivity's PDF was well fitted by a gamma distribution. In Fig. 5, a random sub-sample of 25% of the overall population of windows is plotted. Although, the distribution does not fit well for reflectivity values below 19 dBZ, the contribution of this precipitation (less than 0.1 mm/h) can be ignored in comparison with the heavy rainfall recorded.

Adapting the Z/R relationship to different rain types within a given storm or event seems to be a promising way to improve radar QPE (Lee and Zawadzki, 2005). Rosenfeld et al. (1995) improved the accuracy of WPMM-estimated rainfall by means of objective classification criteria based on parameters such as freezing level or bright-band fraction. In the present work, the classification criteria developed by Biggerstaff and Listemaa (2000) were performed within a 3D scheme to recognise convective/stratiform areas based on a previous study (Steiner et al., 1995). These algorithms distinguish between convective and stratiform areas according to reflectivity thresholds and gradients within different CAPPI levels, which were regionalised to Catalonia by Rigo and Llasat (2004). According to this methodology, in the present study, each different subset of every window was counted in different groups. Therefore, for the same rain gauge intensity window, two radar reflectivity windows are set. This approach to the classification criteria results in an ambiguous rain gauge probability distribution function. The ambiguous relation between the intensity and rain type should be subsequently calculated as two independent unambiguous datasets.

Using both parametric and non-parametric techniques, the derivation of the Z/R relation is very simple and straightforward. A randomisation process is applied by selecting different sizes of sub-samples to ensure the minimisation of spatial and geometric errors. This process also provides probabilistic information about the convergence of the population to a final relationship. In this way, the standard deviation (SD) is used to evaluate the consistency of the new relation and the range over which the final relation is absolutely sound.

4.1.2 Advection correction

The temporal sampling effect of radar observations can lead to significant errors in the estimated accumulated rainfall as shown in several studies (Liu and Krajewski, 1996; Fabry et al.,

1994). To correct this source of error, Anagnostou and Krajewski (1999) proposed an advection correction method based on cross-correlation maximisation (Rinehart and Garvey, 1978). This procedure could be applied not only to correct this rainfall estimation, but also to increase the time resolution. For this reason, instead of calculating the cross-correlation coefficient between the two whole images, the first image is divided into a number of template tiles (Fig. 6a). Each template window will be searched for in the second image using a search window (dashed line in Fig. 6a and 6b), whose size depends on the maximum storm speed that is expected between two sequential images. In the present work, this technique was used to obtain the advective displacement vector (vector in Fig. 6b). This displacement (p, q) indicates a storm or cell movement (Dransfeld et al., 2006).

Once the advective displacement vector has been obtained by this method, a shape morphology transformation is performed by means of temporal weights based on a more complex shape transformation (Turk and O'Brien, 2005). Both the first and second images are extrapolated by means of the computed velocity to the same temporal interval. Then, the pixel value is calculated as the temporal-weighted sum of the two images as shown in the next function:

$$R(x, y, t) = \frac{1}{T^2} \cdot \sum \left\{ (T - t) \cdot \widetilde{A}(t) + t \cdot \widetilde{B}(t) \right\} \tag{6}$$

where the transformed field $\widetilde{A}$ and $\widetilde{B}$ are calculated as a time function by

$$\widetilde{A}(t) = A[x - \frac{t}{T} \cdot c \cdot \cos\theta, y - \frac{t}{T} \cdot c \cdot \sin\theta] \tag{7}$$

$$\widetilde{B}(t) = B[x + \frac{T - t}{T} \cdot c \cdot \cos\theta, y + \frac{T - t}{T} \cdot c \cdot \sin\theta] \tag{8}$$

where c is the advective velocity [km/h] and θ is the displacement angle. t is the time and T [hour] represents the original time resolution of radar.

The template size selected is 10x8 pixels, whereas the search window for the second image is 16x14 pixels. This size was calculated by taking into account a maximum storm movement lower than 140 km/h following the works of Steinacker et al. (2000) and Rigo (2004). Fig 7 shows the downscaling from 6 minutes to 1 minute.

4.1.3 Rainfall data into RIBS Hydrological model

The RIBS model requires that rainfall input data be mapped to the rectangular grid of the DEM. As radar images and DEM resolutions are different and may correspond to different projections, a preliminary treatment of radar images is required.

The main step is an interpolation to downscale the radar resolution grid (2 km $\times$ 2 km) to the DEM resolution (200 m $\times$ 200 m). The easiest and quickest way is to perform an ordinary linear interpolation, but this methodology does not exactly preserve the total amount of precipitation over the whole domain due to mismatching grids (Fig. 8). To avoid this, another procedure was developed in the present work. As shown in Fig. 8, some DEM grid cells are divided into two different reflectivity parts (grey cell). The main purpose of the new procedure is to preserve the total areal precipitation amount, which is achieved by an area-weighted interpolation. This could be formulated in a general way as follows:

$$R_f = \frac{\sum \text{Subarea}_{\text{pixel}_i} \cdot R_{\text{pixel}_i}}{\text{Area DEM grid pixel}} \tag{9}$$

Once rain rated for every cell of the whole domain has been calculated by this area-weighted interpolation, the Besòs Basin shape is cut out from the high resolution rainfall image.

4.1.4 Radar rainfall validation

To evaluate the accuracy of the radar rainfall estimation, three error indexes are calculated. The first one is the log ratio bias (10), which is a relative error and provides information about the total amount of precipitation:

$$\text{logratiobias} = \log \cdot \frac{\sum \cdot R_i}{\sum \cdot P_i} \tag{10}$$

The second is the Root Mean Square Error (11) [mm], which determines the accuracy of the estimation gauge by gauge.

$$\text{RMSE} = \sqrt{\frac{\sum (R_i - P_i)^2}{n_i}} \tag{11}$$

The third is the Mean Error (12) [mm], which defines whether the rainfall is under/over-estimated.

$$\text{ME} = \frac{\sum (R_i - P_i)}{n_i} \tag{12}$$

where R_i and P_i are the daily rainfall accumulations derived from the radar and registered by SMC rain gauges, respectively.

4.2 Hydrological Modeling.

4.2.1 Selection of rainfall time resolutions

Spatially distributed precipitation maps can be constructed for each event by summing the new advected radar rainfall estimation with a time resolution of 1 minute. A set of time resolutions must be selected to perform the analysis.

The required minimum time resolution of rainfall for Mediterranean regions can be estimated as a function of the basin area (Eq. 13), taking into account that time resolutions higher than 3 minutes only become relevant for basin areas smaller than 10 ha (0.1 km^2) (Berne et al., 2004).

$$\Delta t = 0.75 \cdot S^{0.3} \tag{13}$$

where Δt is the required minimum time resolution [min], and S is the basin area [ha].

4.2.2 Probabilistic Calibration.

The distributed RIBS model was calibrated using a probabilistic approach based on a multiobjective calibration methodology, since both different aspects of the hydrograph and the uncertainty in the hydrologic model estimations may be taken into account. The calibration result is a probability density function, which represents each calibration model parameter (Mediero et al., 2011).

The probabilistic calibration methodology can be summarised as follows. First, a sensitivity analysis was performed over the parameters of the RIBS model. The observed rainfall data in the first event for 15 minutes of time resolution was given as model input, and model parameter values were randomised from uniform distributions. A modification of the Generalised Sensitivity Analysis (GSA) methodology proposed by Freer et al. (1996) was applied. This analysis showed that the most influential parameters in the model output are as follows: the rate of variation of the hydraulic conductivity in depth (f), the soil anisotropy coefficient (α), the ratio of hillslope flow velocity to channel flow velocity (K_v) and the coefficient of the law that relates hillslope flow velocity to discharge in the basin outlet (C_v).

Second, the proper calibration methodology was performed over the first three recorded events for each rainfall time resolution. A large set of synthetic hydrographs was generated by repetitive simulations of the RIBS model; these simulations generated randomised sets of values for the most influential model parameters, which were identified in the first step. As the model utilisation is the prediction of flash floods, the Root Mean Square Error (RMSE), Mean Absolute Error (MAE) and Nash-Sutcliffe Efficiency Coefficient (NSE) were selected as objective functions to conduct the multiobjective calibration.

In a multiobjective calibration, no single solution can minimise all of the objective functions at the same time (Gupta et al., 1998). Therefore, the Pareto solutions were identified to determine the set of non-inferior solutions (Yapo et al., 1998). Each calibration model parameter was represented by a probability density function (pdf) fitted from the set of Pareto solutions in the three calibration events. The distribution functions that best fit the variability of each parameter were identified by means of traditional goodness-of-fit tests, i.e. Chi-Squared test and Kolmogorov-Smirnov test.

4.2.3 Sensitivity analysis of the rainfall time resolution

The result of the probabilistic calibration of the RIBS model is a pdf for each parameter, which represents each parameters variability. Therefore, the result of the model calibration is not a single hydrograph, but an ensemble distribution of discharges at each time step. This ensemble is obtained by the randomisation of the model parameter values with the calibration results. The number of hydrographs used in the time resolution analysis must be large enough to reach the stabilisation of the model results. The required number of simulations was defined through a sensitivity analysis, which established that 200 model simulations were required to obtain reliable results.

A sensitivity analysis of the rainfall time resolution was performed over the last observed event. Differences between the simulated set of hydrographs and the observed hydrograph were quantified by four measures. RMSE and MAE were selected to measure the accuracy of the simulations (14–15).

$$\mathrm{RMSE} = \sqrt{\frac{1}{T_s} \cdot \sum_{t=1}^{T_s} \left(Q_o^t - Q_s^t\right)^2} \tag{14}$$

$$\mathrm{MAE} = \sum_{t=1}^{T_s} \left(Q_o^t - Q_s^t\right) \tag{15}$$

Two other measures were added to improve the assessment. The estimation bias was quantified by the Nash-Sutcliffe global efficiency index (R^2 ($\mathrm{MQ}_{0.5}$) (Eq. 16), which measures the utility of the median as a forecast (Xiong and O'Connor, 2008). The predictive capability of the calibrated model was quantified by the Containing Ratio (CR) (Eq. 17), which measures the number of observations that fall within the prediction intervals linked to a given confidence level (Montanari, 2005).

$$R^2(\mathrm{MQ}_{0.5}) = 1.0 - \frac{\sum_{t=1}^{T_s}[Q_0^t - \mathrm{MQ}_{0.5}^t]^2}{\sum_{t=1}^{T_s}[Q_0^t - \overline{Q_0}]} \tag{16}$$

where Q_o^t is the observed discharge at time t, Q_s^t is the simulated discharge at time t, $\overline{Q_o}$ is the mean of observed discharges in the event, $\mathrm{MQ}_{0.5}^t$ is the median of simulated discharges at time t and T_s is the total number of time steps.

$$\mathrm{CR}(\alpha) = \frac{\sum I[Q_0^t]}{T_s} \tag{17}$$

where $I[Q_0^t]$ is equal to 1 if the observed discharge at time t holds between the confidence interval, and α is the confidence level, which was set at 10%.

5 Results

5.1 WPMM methodology

The four selected heavy rainfall events were produced by very different meteorological events. For this reason, the calibration method previously presented was applied for each case such that eight Z/R relations were obtained: two fitting methods for each of the four case studies. In the next table (Table 4), the eight power-law functions were tested for every case.

Regarding the comparison of both methodologies, it can be observed that a parametric fit improves the results compared to a non-parametric fit (Fig. 9). The left box plot for a given fitting methodology represents the results for the Z/R obtained for the same study case, whereas the right box plot shows the Z/R results computed for the three other case studies. The log ratio bias and the RMSE show better results for both box plot regarding the mean and the IQ range. It could be observed that, for the most part, the most suitable data for the calibration are our own case data. Nevertheless, as the results show, the calibration could be performed by using data from other cases that achieve accurate precipitation estimations.

A comparison between both methodologies shows that the parametric fit improves the range of applicability of the new Z/R relationship. It can be observed in figure 10 that the SD is higher for the tails of the non-parametric Z/R relation (Fig. 10a) than for the parametric Z/R relation(Fig. 10b). This is caused by the scarcity of values at the tails of the probability distribution function for the reflectivity and high intensity rainfall values. The parametric fit does not have this problem because it has only two parameters to compute, and this computation gives more weight to the central values of the distribution.

5.2 Advection correction

In the next table (Table 5), the results of applying the advection technique to the best rainfall estimation method are shown. The use of a cross-correlation technique to interpolate the rain improved the results previously obtained for the root mean square error and mean error for all of the cases; however, it did not change the total radar rainfall field.

The impact of the advection can be observed in figure 11. The maximum values and the shape of the rainfall field has changed. Regarding the improvement in the hourly accumulated rainfall, figure 12 compares the log ratio bias and the RMSE of the QPE before and after applying the advection correction technique.

5.2.1 Selection of rainfall time resolutions

The minimum time resolution for the gauge stations in the Besòs Basin calculated using Eq. 13 are included in Table 2. It can be seen that they are within 12 to 24 minutes. Therefore, the calibration of the RIBS model was performed for six time resolutions: 30, 24, 18, 15, 12 and 6 min. Resolutions higher than 6 min were not considered because they highly increase the computation times of the RIBS model. Moreover, these time resolutions are not relevant for the basin areas considered in the Besòs Basin.

5.3 Hydrologic model calibration

The distributed RIBS model was calibrated in the Besòs Basin with the first three observed events. The basin shape and the locations of the gauging stations are shown in Fig. 2, and their basic properties are presented in Table 2. The model was calibrated using data from the Gramenet station, very near the basin outlet. Spatially distributed precipitation maps were constructed for each event by summing the new advected radar rainfall estimation for 30, 24, 18, 15, 12 and 6 min. The antecedent moisture content was used as an input in the RIBS model and was estimated from rainfall and temperature data in the days before the flood event.

The calibration methodology was conducted for each rainfall time resolution to take into account the fact that some hydrological parameters may be dependent on the time scale. The calibration results are summarised by the main statistics of the distribution of parameter values for each time resolution (Table 3).

5.4 Sensitivity to precipitation time resolution

A sensitivity analysis of the rainfall time resolution was carried out with the last event at each of the six gauging stations: Lliça station on the Tenas River, Montcada Station on the Ripoll River, just upstream of its confluence with the Besòs River, Gramenet Station on the Besòs River, very near the basin outlet, Garriga Station on the Congost River, Mogent Station on the Mogent River and Mogoda Station on the Caldas River (Fig. 2).

A set of 200 simulated hydrographs was generated for each time resolution. These simulated hydrographs were compared with the observed flows for each gauge with the measures described in the subsubsectionSensitivity analysis of the rainfall time resolution; the obtained results are presented in Table 6 and Figs. 13 and 14.

The predictive capability for peak discharge with a significance level of 10% is presented as a function of rainfall time resolution (Fig. 13). The range between confidence limits is represented by the length of the error bars. Most stations show the least variability and the best fit between the median and the observed value for time resolutions of 12, 15 and 18 min. In general, both the width of the confidence intervals and the distances between the median and the observed peak increase as the rainfall time resolution deviates from these values, reaching the maximum at the most extreme time resolutions, i.e., 6 and 30 min. The largest deviations of the median from the observed peak at most stations are also at 6 and 30 min.

The results obtained for the four validation measures are shown in Fig. 14. To allow for the comparison among gauges, RMSE and ME were standardised by the observed peak discharge. As shown in Fig. 14a, the minimum RMSE is reached at all stations except Mogoda for 15 min. The model performance is maintained for time resolutions below 12 min but decreases sharply for time resolutions above 18 min in the case of the smaller stations, Mogoda, Lliça and Garriga. This finding shows that time resolutions smaller than 15 minutes worsen the hydrological results for the basins with smaller areas.

The absolute value of the bias reaches the minimum for time resolutions of 12 and 15 min, the differences between these two time resolutions being small. The bias shows the same trend as the RMSE for the smaller basins as it decreases the model performance as the time resolution

decreases. This finding indicates that time resolutions higher than 15 minutes worsen the hydrological results for Mogoda, Lliça and Garriga basins. Although Fig. 14b presents the absolute value of the bias, in general, the bias is positive for time resolutions smaller than 15 min and negative for the rest.

Gramenet, Montcada and Mogent Stations clearly reach the best $R^2(\mathrm{MQ}_{0.5})$ for a time resolution of 15 min. Mogoda and Lliça Stations reach the maximum for 15 min, but there are no large differences from the result for 12 min. Garriga reaches the maximum for 12 min. These results indicate that the larger basins produce better results for a time resolution of 15 minutes and that the smaller basins produce better results for a higher time resolution closer to 12 minutes.

The behaviour of CR shows that most stations reach the maximum for 15 min, except for Lliça, where the maximum corresponds to 12 min. The larger basins (Mogent, Montcada and Gramenet) show a sharp decrease in model performance as the time resolution increases. The best results are achieved for 15 min, but the results for 12 minutes are worse than those for 18 min. This finding indicates that the results for the larger worsen at time resolutions higher than 15 minutes. In the case of smaller basins, there are not relevant differences between time resolutions of 12 and 15 minutes.

It seems that the decrease in model performance with a decrease in time resolution may depend on the maximum time resolution required to characterise the rainfall variability in time. The decrease in model performance for time resolutions higher than 15 min could be due to the minimum time resolution required for the hydrological model to characterise the runoff processes. This resolution seems to be a threshold for a basin area of 150 km^2. Basins with areas below this threshold produce better results with a time resolution of 12 minutes, causing the model performance to decrease sharply as the time resolution decreases. Basins with areas higher than 150 km^2 achieve better results with a time resolution of 15 minutes.

These results indicate that 15 min is the best rainfall time resolution for basins larger than 150 km^2 in the Besòs Basin and 12 min is the best resolution for basins smaller than 150 km^2. These time resolutions provide a good representation of the rainfall characteristics of the Besòs River basin as well as allow for a good simulation of the hydrological processes that occur in

the area.

6 Discussion and conclusions

Distributed hydrological models improve the simulation of convective rainfall events, as they can accept spatially distributed rainfall maps as input data. Because of this, an effort was made to couple radar data with a distributed hydrologic model to simulate flash-flood events recorded in Catalonia.

This contribution provides a good example of the numerous problems that exist in QPE. First, the traditional Z/R power-law relationships have not worked well when applied to the selected cases. It is difficult to determine with certainty whether this problem might be associated with poor calibration or maintenance of the radar network or with the attenuation caused by heavy precipitation. To obtain a suitable QPE, a Window Probability Matching Method (WPMM) and an advection correction were applied in this work.

The results show that the proposed methodology represents a good improvement in radar rainfall estimation. Furthermore, despite the dependence of the WPMM on the selected probability distribution fitting function, it has been shown that rainfall estimation improves with the two tested functions. Accordingly, it is interesting that the minimum root mean square error is obtained by fitting parametric functions. Initially, the empirical pdf was tested to reproduce exactly the original WPMM technique. However, the results - not only in the lower tail of the distribution, but also in the higher reflectivity tail - show poor stability over the SD test. For this reason, a smooth non-parametric technique (Kernel smooth pdf) was tested. The results improve slightly, but the stability is not sufficiently high. For this reason, several parametric functions were tested.

The best-fitting parametric functions used were a gamma function for reflectivity and an exponential function for rainfall intensity. Gamma functions have a potential factor multiplied by an exponential function. Because the exponential function does not have the potential factor, the linear relationship between rainfall intensity and reflectivity produces a curve of order k along the logarithmic axis. The result of this linear relationship between the two different functions

is a non-power-law relation for the transformation of reflectivity into rainfall intensity, which increases the quantitative precipitation estimation due to the convex shape of the WPMM function in the semilog rainfall intensity – reflectivity axis. On the other hand, the smallest bias is usually obtained by fitting with a non-parametric kernel function. In this methodology, both the rainfall and reflectivity values are fitted using the same function. Moreover, this function is not parametric but is built by a convolution of Gaussian functions. Thus, the final Z/R shape relation does not have a predefined form due to the linear relation of the function, as occurs with parametric functions. The shape obtained by this method is probably the classic power-law relation. Comparing both methodologies, the parametric function provides an increase in lower reflectivity values and a decrease in higher values, whereas the non-parametric methodology produces a similar shape, though it is displaced to the right, which causes the rainfall intensity to increase for all reflectivity values. The second correction made by WPMM non-parametric methodology could be related to the underestimation of the reflectivity due to the power parameter calibration or own rainfall attenuation.

Taking into account the improvement that involves a convective/stratiform distinction, two Z/R relations are obtained. This new QPE method produces better results for the BIAS index, which indicates a decrease of the total rainfall field. Furthermore, the new WPMM Z/R relation shape is less convex than the previous one. Accordingly, this approach should be useful for obtaining better QPE results if more in-depth rain regime research was performed.

After that, an advection correction was applied to correct the rainfall amount. This correction was based on the hypothesis that rainfall intensity is a field in continuous variation. This method is applied in several meteorological services to accumulate rainfall over a period of one hour. In the present work, this technique was applied to every six radar rainfall fields with two objectives. The first was to improve the total rainfall estimation; the second was to increase the temporal resolution to feed the hydrological model. By applying this method, the root mean square error decreased, although the bias did not show this behaviour. The cause of this could be the significance of each improvement. The root mean square error is more closely related with point errors, whereas the bias is mainly related to the entire rainfall field.

Comparing the results obtained in the literature for the Z/R relations (Atencia et al., 2008)

with the results of the combined application of both methodologies, the RMSE has been reduced by up to 40% and log ratio bias between 75% and 95%. These accurate results allow us to couple radar rainfall information across an area-weighted interpolation.

Once a more accurate rainfall field was obtained for each 6-minute interval, it was taken as input data for the hydrologic model. Due to the fact that the calibration of distributed hydrological models is strongly dependent on the time resolution of rainfall data, the advection correction method based on a cross-correlation technique was applied to implement a temporal disaggregation at several time resolutions (30, 24, 18, 15, 12, 6 and 2 min). Time resolutions higher than 6 min lead to both unaffordable computation times for operational hydrological forecasting and irrelevant time resolutions for the gauging stations in the Besòs River Basin. Accordingly, only the six highest time resolutions were compared.

A probabilistic calibration methodology was applied to three flood events to obtain the probability density functions that best represent the variability of each model parameter. A sensitivity analysis of the rainfall time resolution was performed for the last event. This sensitivity analysis showed that basins with areas below 150 km2 provide better results with a time resolution of 12 minutes, and basins with areas higher than 150 km2 achieve better results with 15 minutes of time resolution. The selected rainfall time resolutions compare well with the results presented by (Berne et al., 2004), who studied urban basins up to 100 km^2 and found a strong relationship between basin size and the minimum required rainfall spatial and temporal resolutions, suggesting a rainfall minimum temporal resolution of 12 min. The basins analysed in this work range from 100 to 1000 km^2 and present an optimum time resolution between 12 and 15 min. The results also suggest a lower dependence of rainfall resolution on basin size for the range analysed, which could also be extrapolated to larger basins.

This work proves that the highest available rainfall time resolution does not necessarily provide the best results in terms of the predictability of peak flow while the radar system is coupled with a distributed hydrologic model. For the optimum time resolution of 15 min, an RMSE average improvement of 16% was obtained for all sub-basins analysed when compared to the 6 min time resolution case, which produced values larger than 10% for all individual basins. The results for other basins could vary across the Mediterranean due to the dependence of the basin

response on other characteristics not analysed in this work, such as geomorphology, geology and vegetation.

Acknowledgements. This research is supported by the Sixth Framework Programme European Commission FLASH project (n.036852). It is also included in the framework of the Spanish Severus project (CGL2006-13372-CO2-02). The authors thank Meteocat (Catalan Meteorological Service) for the rainfall data from the XAC and XMET networks and the radar data from the XRAD network. The authors also thank ACA (Catalan Agency of Water) for the rainfall and stream flow data from the SAIH network. Additionally, the authors would like to thank CLABSA for the Besòs Basin information.

References

Anagnostou, E. and Krajewski, W.: Real-time radar rainfall estimation. Part I: Algorithm formulation, Journal of Atmospheric and Oceanic Technology, 16, 189–197, doi:10.1175/1520-0426(1999)016⟨0189:RTRREP⟩2.0.CO;2, 1999.

Arnaud, P., Bouvier, C., Cisneros, L., and Dominguez, R.: Influence of rainfall spatial variability on flood prediction, Journal of Hydrology, 260, 216–230, doi:10.1016/S0022-1694(01)00611-4, 2002.

Atencia, A., Ceperuelo, M., Llasat, M., and Vilaclara, E.: A new non power-law Z/R relation in western Mediterranean area for flash-flood events, in: Proceedings of Fifth European Conference on Radar in Meteorology and Hidrology (ERAD)., p. 14, Helsinki, Finland, 7, 2008.

Atlas, D., Rosenfeld, D., Wolff, D., Aeronautics, N., and Space Administration. Goddard Space Flight Center, Greenbelt, M.: Climatologically tuned reflectivity-rain rate relations and links to area-time integrals, Journal of Applied Meteorology, 29, 1120–1135, 1990.

Barnolas, M. and Llasat, M. C.: A flood geodatabase and its climatological applications: the case of Catalonia for the last century, Natural Hazards and Earth System Science, 7, 271–281, 2007.

Bech, J., Codina, B., Lorente, J., and Bebbington, D.: The sensitivity of single polarization weather radar beam blockage correction to variability in the vertical refractivity gradient, Journal of Atmospheric and Oceanic technology, 20, 845–855, doi:10.1175/1520-0426(2003)020⟨0845:TSOSPW⟩2.0.CO;2, 2003.

Bell, V. and Moore, R.: The sensitivity of catchment runoff models to rainfall data at different spatial scales, Hydrology and Earth System Sciences, 4, 653–667, 2000.

Berne, A., Delrieu, G., Creutin, J., and Obled, C.: Temporal and spatial resolution of rainfall measurements required for urban hydrology, Journal of Hydrology, 299, 166–179, 2004.

Biggerstaff, M. and Listemaa, S.: An improved scheme for convective/stratiform echo classification using radar reflectivity, Journal of Applied Meteorology, 39, 2129–2150, doi:10.1175/1520-0450(2001)040⟨2129:AISFCS⟩2.0.CO;2, 2000.

Carpenter, T. and Georgakakos, K.: Intercomparison of lumped versus distributed hydrologic model ensemble simulations on operational forecast scales, Journal of Hydrology, 329, 174–185, doi:10.1016/j.jhydrol.2006.02.013, 2006.

Ceperuelo, M. and Llasat, M.: La Precipitacion Convectiva en las Cuencas Internas de Catalunya, Revista del Aficionado a la Meteorologıa, 23, 2004.

Corral, C., Sempere-Torres, D., and Berenguer, M.: A distributed rainfall runoff model to use in Mediterranean basins with radar rainfall estimates, in: 30 Conf. on Radar Meteor, pp. 6–8, 2001.

Delrieu, G., Andrieu, H., and Creutin, J.: Quantification of path-integrated attenuation for X-and C-band weather radar systems operating in Mediterranean heavy rainfall, Journal of Applied Meteorology, 39, 2000.

Dransfeld, S., Larnicol, G., and Le Traon, P.: The Potential of the Maximum Cross-Correlation Technique to Estimate Surface Currents From Thermal AVHRR Global Area Coverage Data, IEEE Geoscience and Remote Sensing Letters, 3, 508–511, doi:10.1109/LGRS.2006.878439, 2006.

Fabry, F., Bellon, A., Duncan, M., and Austin, G.: High resolution rainfall measurements by radar for very small basins: the sampling problem reexamined, Journal of Hydrology, 161, 415–428, 1994.

Franco, M., Sánchez-Diezma, R., and Sempere-Torres, D.: Improving radar precipitation estimates by applying a VPR correction method based on separating precipitation types, in: Proceedings of Fifth European Conference on Radar in Meteorology and Hidrology (ERAD)., p. 14, Helsinki, Finland, 14, 2008.

Freer, J., Beven, K., and Ambroise, B.: Bayesian estimation of uncertainty in runoff prediction and the value of data: An application of the GLUE approach, Water Resources Research, 32, 2161–2173, 1996.

Garrote, L. and Bras, R.: A distributed model for real-time flood forecasting using digital elevation models, Journal of Hydrology, 167, 279–306, doi:10.1016/0022-1694(94)02592-Y, 1995a.

Garrote, L. and Bras, R.: An integrated software environment for real-time use of a distributed hydrologic model, Journal of Hydrology, 167, 307–326, 1995b.

Garrote, L., Molina, M., and Mediero, L.: Hydroinformatics in Practice: Computational Intelligence and Technological Developments in Water Applications, chap. Learning Bayesian networks from deterministic rainfall–runoff models and Monte-Carlo simulation, pp. 375–388, Springer, doi:10.1007/978-3-540-79881-1_27, 2007.

Gupta, H., Sorooshian, S., Yapo, P., et al.: Toward improved calibration of hydrologic models: Multiple and noncommensurable measures of information, Water Resources Research, 34, 751–763, 1998.

Haddad, Z., Short, D., Durden, S., Im, E., Hensley, S., Grable, M., and Black, R.: A new parametrization of the rain drop size distribution, IEEE Transactions on Geoscience and Remote Sensing, 35, 532–539, doi:10.1109/36.581961, 1997.

Kaplan, E. and Meier, P.: Nonparametric estimation from incomplete observations, Journal of the American statistical association, 53, 457–481, doi:10.2307/2281868, 1958.

Krajewski, W., Lakshmi, V., Georgakakos, K., and Jain, S.: A Monte Carlo study of rainfall sampling effect on a distributed catchment model, Water resources research, 27, 119–128, doi:10.1029/90WR01977, 1991.

Lee, G. and Zawadzki, I.: Variability of drop size distributions: Time-scale dependence of the variability and its effects on rain estimation, Journal of Applied Meteorology, 44, 241–255, doi:10.1175/JAM2183.1, 2005.

Liu, C. and Krajewski, W.: A comparison of methods for calculation of radar-rainfall hourly accumulations, Journal of the American Water Resources Association, 32, 305–315, doi:10.1111/j.1752-1688.1996.tb03453.x, 1996.

Llasat, M., Rigo, T., and Barriendos, M.: The Montserrat-2000 flash-flood event: a comparison with the floods that have occurred in the northeastern Iberian Peninsula since the 14th century, International Journal of Climatology, 23, 453–469, doi:10.1002/joc.888, 2003.

Llasat, M. C., López, L., Barnolas, M., and Llasat-Botija, M.: Flash-floods in Catalonia: the social perception in a context of changing vulnerability, Advances in Geosciences, 17, 63–70, 2008.

Madsen, H.: Parameter estimation in distributed hydrological catchment modelling using automatic calibration with multiple objectives, Advances in Water Resources, 26, 205–216, doi:10.1016/S0309-1708(02)00092-1, 2003.

Marshall, J. and Palmer, W.: The distribution of raindrops with size, Journal of the Atmospheric Sciences, 5, 165–166, doi:10.1175/1520-0469(1948)005⟨0165:TDORWS⟩2.0.CO;2, 1948.

Mediero, L., Garrote, L., and Martin-Carrasco, F.: A probabilistic model to support reservoir operation decisions during flash floods/Un modele probabiliste d'aide a la decision pour la gestion d'un reservoir lors de crues eclairs, Hydrological Sciences Journal/Journal des Sciences Hydrologiques, 52, 523–537, doi:10.1623/hysj.52.3.523, 2007.

Mediero, L., Garrote, L., and Martn-Carrasco, F.: Probabilistic calibration of a distributed hydrologic model for flood forecasting, Hydrological Sciences Journal, p. In Press, 2011.

Montanari, A.: Large sample behaviors of the generalized likelihood uncertainty estimation (GLUE) in

assessing the uncertainty of rainfall-runoff simulations, Water Resour. Res, 41, 2005.

Morin, E. and Gabella, M.: Radar-based quantitative precipitation estimation over Mediterranean and dry climate regimes, Journal of Geophysical Research-Atmospheres, 112, D20 108, doi:10.1029/2006JD008206, 2007.

Morin, E., Enzel, Y., Shamir, U., and Garti, R.: The characteristic time scale for basin hydrological response using radar data, Journal of Hydrology, 252, 85–99, doi:10.1016/S0022-1694(01)00451-6, 2001.

Parzen, E.: On estimation of a probability density function and mode, The Annals of Mathematical Statistics, 33, 1065–1076, doi:10.1214/aoms/1177704472, 1962.

Refsgaard, J.: Parameterisation, calibration and validation of distributed hydrological models, Journal of Hydrology, 198, 69–97, doi:10.1016/S0022-1694(96)03329-X, 1997.

Rigo, T.: Estudio de sistemas convectivos mesoescalares en la zona mediterránea occidental mediante el uso del radar meteorológico, Ph.D. thesis, PhD thesis, University of Barcelona, Internal publication, 2004.

Rigo, T. and Llasat, M.: A methodology of convective structures using meteorological radar: Application to heavy rainfall events on the Mediterranean coast of the Iberian Peninsula, Nat. Hazards Earth Syst. Sci, 4, 59–68, 2004.

Rinehart, R. and Garvey, E.: Three-dimensional storm motion detection by convective weather radar, Nature, 273, 287–289, 1978.

Robinson, J., Sivapalan, M., and Snell, J.: On the relative roles of hillslope processes, channel routing, and network geomorphology in the hydrologic response of natural catchments, Water Resources Research, 31, 3089–3101, doi:10.1029/95WR01948, 1996.

Rosenfeld, D., Wolff, D., and Atlas, D.: General probability-matched relations between radar reflectivity and rain rate, Journal of Applied Meteorology, 32, 50–72, doi:10.1175/1520-0450(1993)032⟨0050:GPMRBR⟩2.0.CO;2, 1993.

Rosenfeld, D., Wolff, D., and Amitai, E.: The window probability matching method for rainfall measurements with radar, Journal of Applied Meteorology, 33, 682–693, doi:10.1175/1520-0450(1994)033⟨0682:TWPMMF⟩2.0.CO;2, 1994.

Rosenfeld, D., Amitai, E., and Wolff, D.: Improved accuracy of radar WPMM estimated rainfall upon application of objective classification criteria, Journal of Applied Meteorology, 34, 212–223, doi:10.1175/1520-0450(1995)034⟨0212:IAORWE⟩2.0.CO;2, 1995.

Sánchez-Diezma, R., Zawadzki, I., and Sempere-Torres, D.: Identification of the bright band through the analysis of volumetric radar data, Journal of Geophysical Research-Atmospheres, 105, 2225–2236,

doi:10.1029/1999JD900310, 2000.

Sánchez-Diezma, R., Sempere-Torres, D., Delrieu, G., and Zawadzki, I.: An improved methodology for ground clutter substitution based on a pre-classification of precipitation types, in: 30 th Internat. Conf. on Radar Meteor, pp. 271–273, Munich, Germany, 2001.

Smith, M., Seo, D., Koren, V., Reed, S., Zhang, Z., Duan, Q., Moreda, F., and Cong, S.: The distributed model intercomparison project (DMIP): motivation and experiment design, Journal of Hydrology, 298, 4–26, doi:10.1016/j.jhydrol.2004.03.040, 2004.

Steinacker, R., Dorninger, M., Wölfelmaier, F., and Krennert, T.: Automatic tracking of convective cells and cell complexes from lightning and radar data, Meteorology and Atmospheric Physics, 72, 101–110, doi:10.1007/s007030050009, 2000.

Steiner, M., Houze Jr, R., and Yuter, S.: Climatological characterization of three-dimensional storm structure from operational radar and rain gauge data, Journal of Applied Meteorology, 34, 1978–2007, doi:10.1175/1520-0450(1995)034⟨1978:CCOTDS⟩2.0.CO;2, 1995.

Turk, G. and O'Brien, J. F.: Shape transformation using variational implicit functions, in: SIGGRAPH '05: ACM SIGGRAPH 2005 Courses, p. 13, ACM, New York, NY, USA, doi:10.1145/1198555.1198639, 2005.

Velasco-Forero, C., Sempere-Torres, D., Sanchez-Diezma, R., Cassiraga, E., and Gomez-Hernandez, J.: A non-parametric methodology to merge raingauges and radar by kriging: sensitivity to errors in radar measurements, in: Proceedings of Third European Conference on Radar in Meteorology and Hidrology (ERAD)., pp. 21–24, Visby, Island of Gotland, Sweden, 2004.

Winchell, M., Gupta, H., and Sorooshian, S.: On the simulation of infiltration-and saturation-excess runoff using radar-based rainfall estimates: Effects of algorithm uncertainty and pixel aggregation, Water Resources Research, 34, 2655–2670, doi:10.1029/98WR02009, 1998.

Xiong, L. and O'Connor, K.: An empirical method to improve the prediction limits of the GLUE methodology in rainfall-runoff modeling, Journal of Hydrology, 349, 115–124, 2008.

Yang, D., Herath, S., and Musiake, K.: Comparison of different distributed hydrological models for characterization of catchment spatial variability, Hydrol. Process, 14, 403–416, doi:10.1002/(SICI)1099-1085(20000228)14:3⟨403::AID-HYP945⟩3.0.CO;2-3, 2000.

Yapo, P., Gupta, H., and Sorooshian, S.: Multi-objective global optimization for hydrologic models, Journal of hydrology, 204, 83–97, 1998.

Zawadzki, I.: On radar-raingage comparison, Journal of Applied Meteorology, 14, 1430–1436, doi:10.1175/1520-0450(1975)014⟨1430:ORRC⟩2.0.CO;2, 1975.

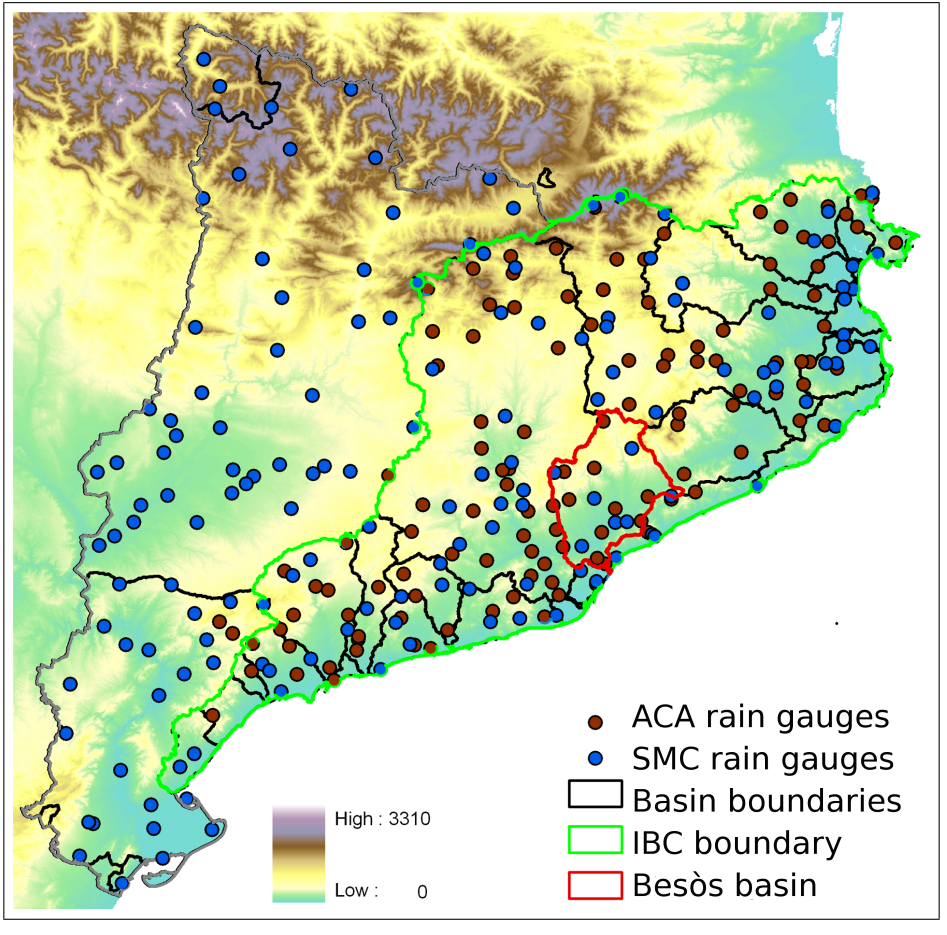

Fig. 1: Boundary of Catalonia with DEM relief. SAIH (ACA rain gauges) and XEMA (SMC rain gauges) networks, with different time resolutions, are shown.

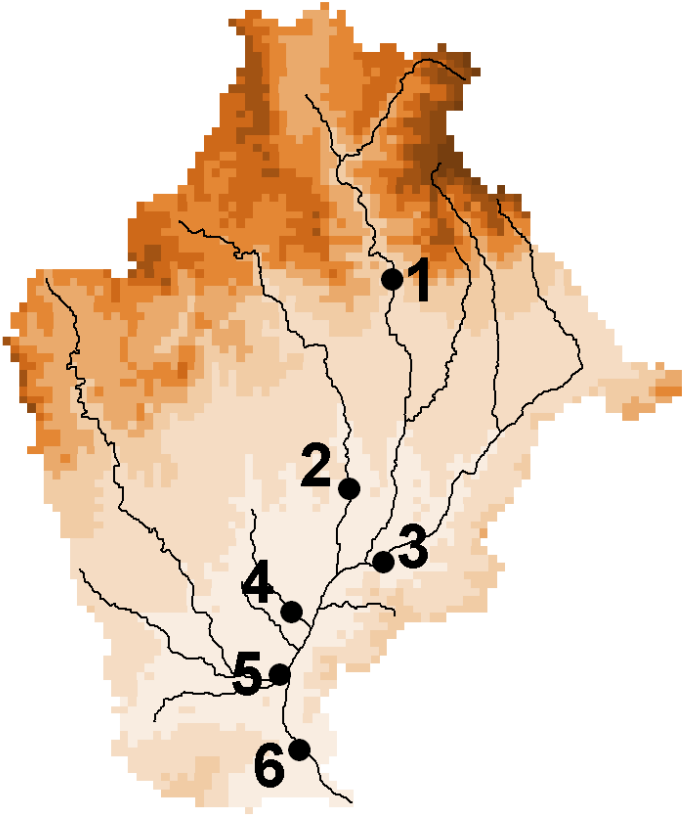

Fig. 2: Location of river gauging stations: 1-Garriga; 2-Lliça; 3-Mogent; 4-Mogoda; 5-Montcada; 6-Gramenet.

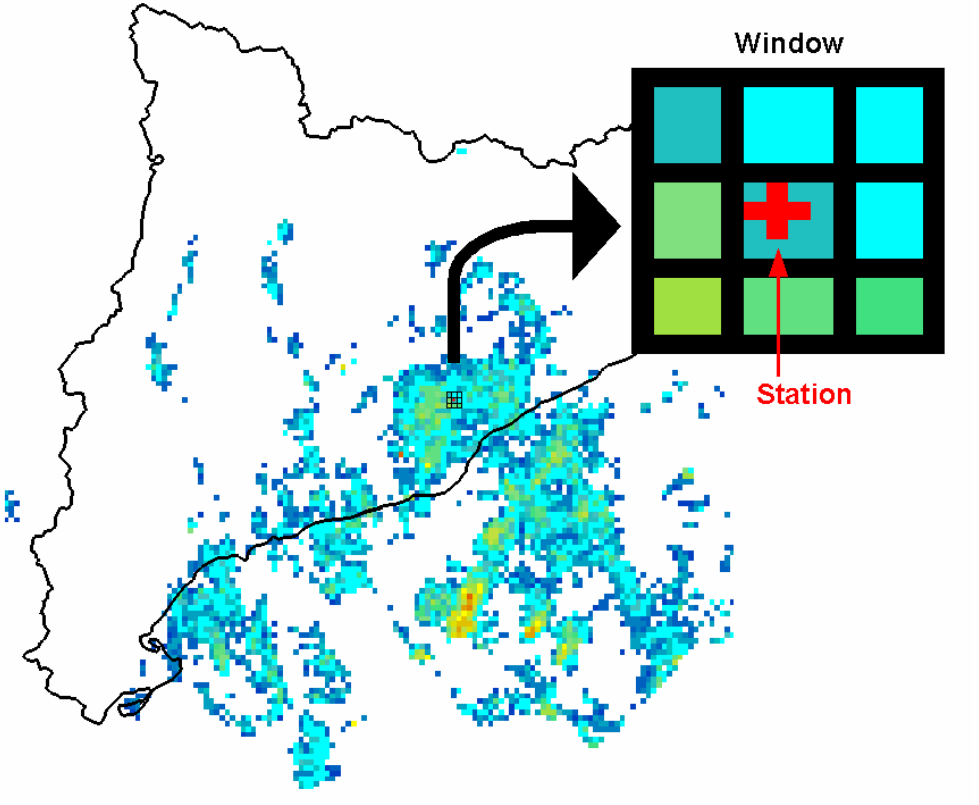

Fig. 3: Radar window example. Square window of 3x3 pixel dimension is centered over a rain gauge (red cross).

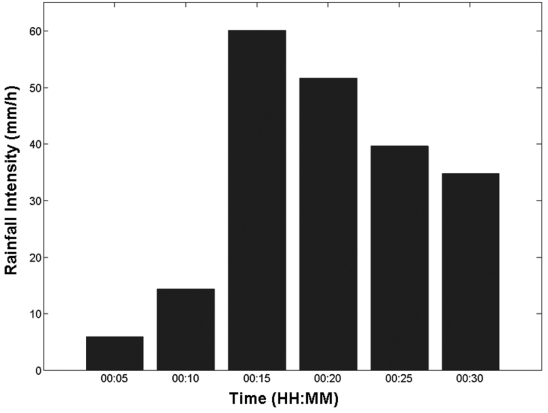

(a) Example of an independent rainfall window dataset: Evolution of 5-minute rainfall rate for a period of 30 minutes.

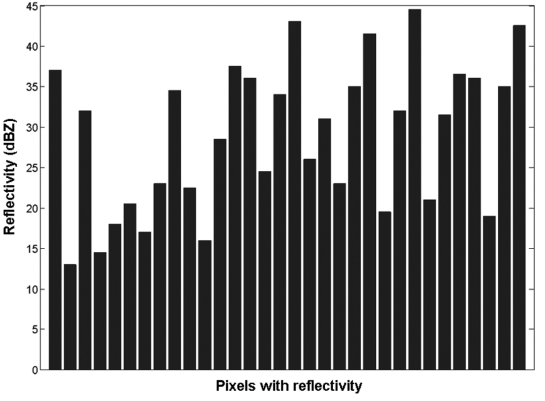

(b) Example of a single independent reflectivity window dataset: 6-minute reflectivities for a period of 30 minutes (5 radar images) and for the nine pixels comprising a window.

Fig. 4: Examples of a rain gauge (a) and reflectivity (b) independent window.

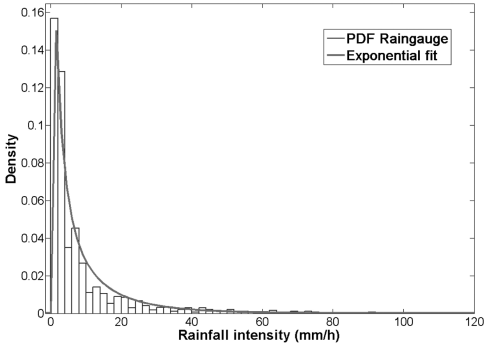

(a)

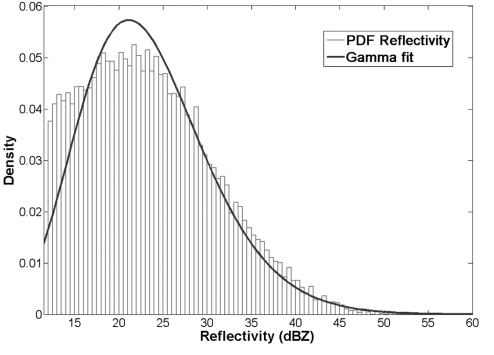

(b)

Fig. 5: The upper picture (a) shows density histogram random sub-sample of 25% of the overall population of rain gauge data and the Exponential PDF fit. The lower one (b) shows density histogram for radar data window and Gamma PDF fit.

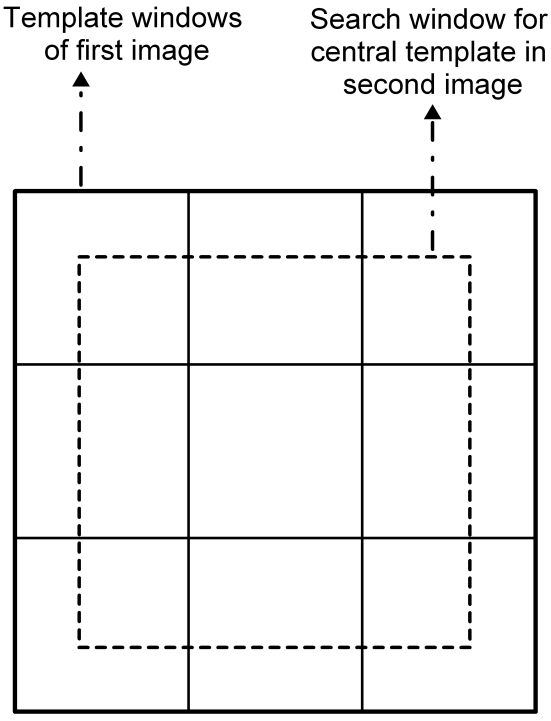

(a) Division of the first image into templates (solid lines) and search area (dashed line) corresponding to the central template.

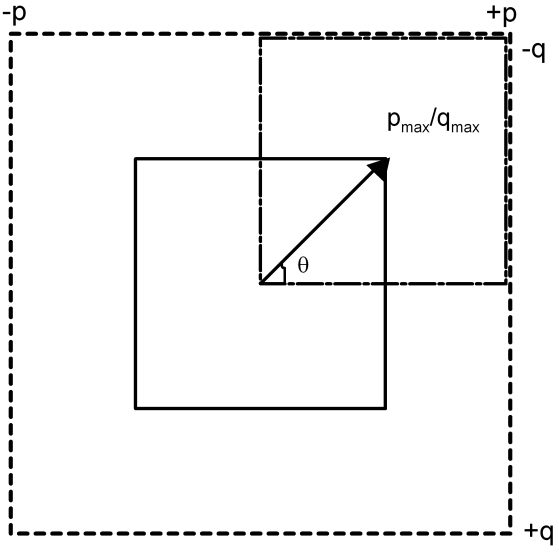

(b) Vector indicating where in the second image the centre of the window (dotted line) closest to the original template (solid line) lies.

Fig. 6: Both pictures, (a) and (b), are extracted from Dransfeld et al. (2006).

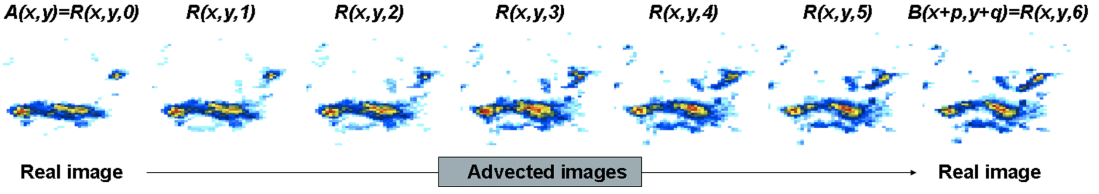

Fig. 7: Real example of radar rainfall disaggregation. In the above example 3x3 templates are shown in each image. The original resolution is 6 minutes and the cross-correlation advection results in a 1 minute resolution.

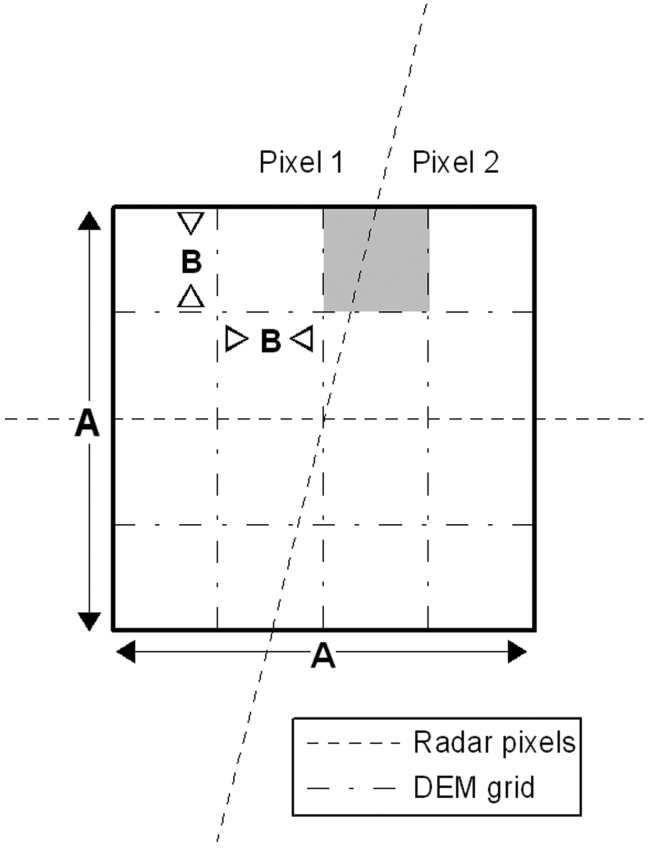

Fig. 8: Superposition of radar pixels over DEM grid over a small domain of area A^2. The highlighted grey DEM grid pixel is used as example of mismatching between the two grids.

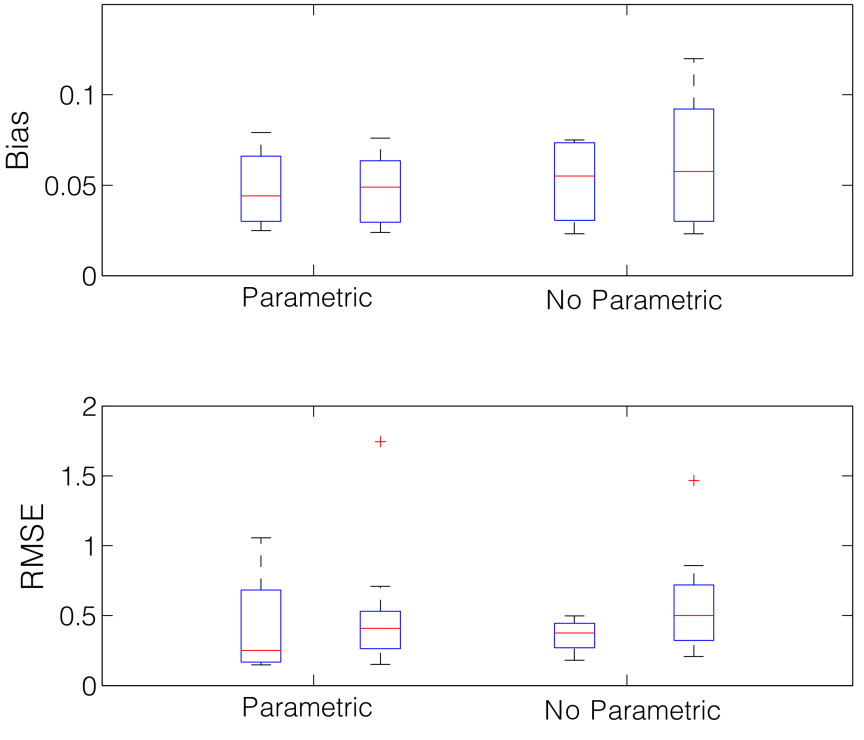

Fig. 9: Box-plot of both fitting techniques (Parametric and non-parametric) for the log ratio bias and the RMSE. The left box-plot for a given fitting methodology represents the results for the Z/R obtained for the same study case whereas the right box plot is the results obtained for the Z/R computed by the three other case studies.

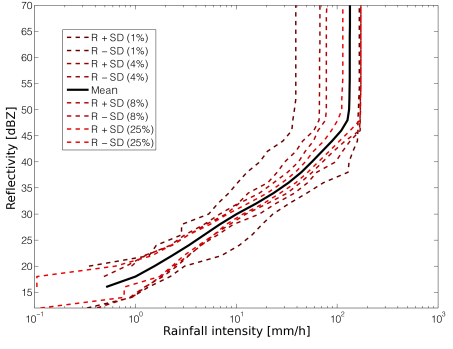

(a) Non-parametric

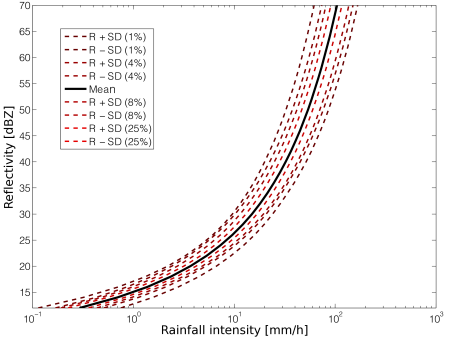

(b) Parametric

Fig. 10: The new Z/R relation (solid middle line), as obtained from WPMM for the full dataset. The broken lines represent plus and minus one standard deviations from the Z/R when calculated by population from 1% to 25% sub-samples. The upper example (a) is the new Z/R relation obtained by non-parametric fitting whereas the lower one (b) correspond to the parametric fit.

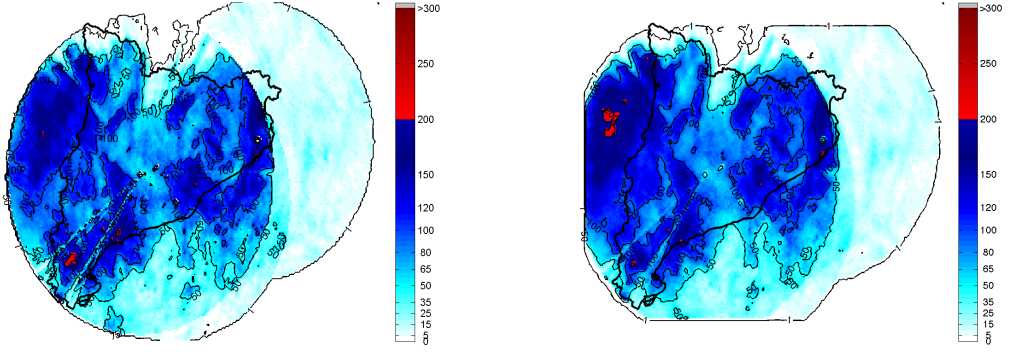

(a) Before adv. correction

(b) After adv. correction

Fig. 11: Comparison between non-advected (a) and advected (b) accumulated rainfall field

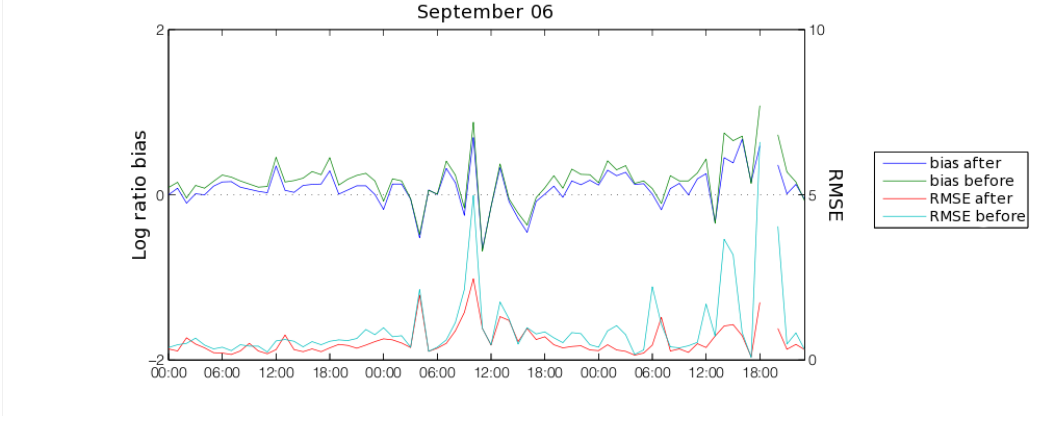

Fig. 12: Validation results for the September 2006 event before and after applying the advection correction.

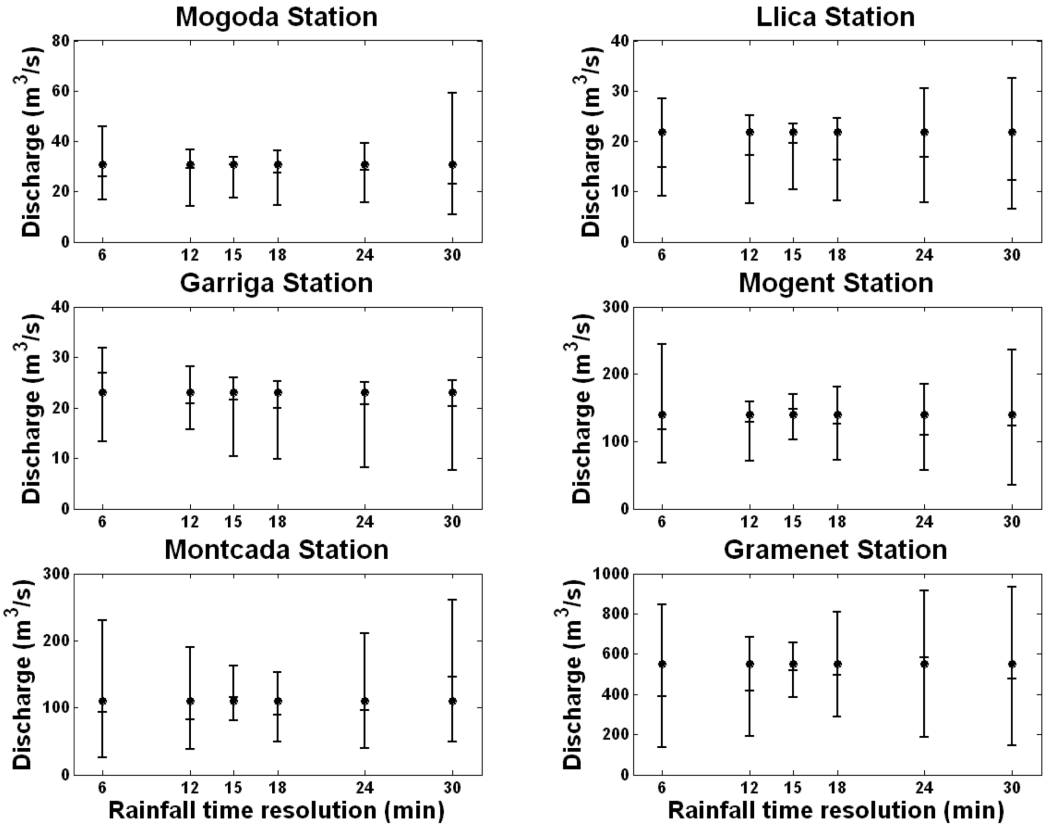

Fig. 13: Validation results for the peak discharge as a function of time resolutions, at all station locations. Observed peak discharge is plotted as solid circle, 5% and 95% percentiles are plotted as vertical bars and the median is plotted as horizontal dash.

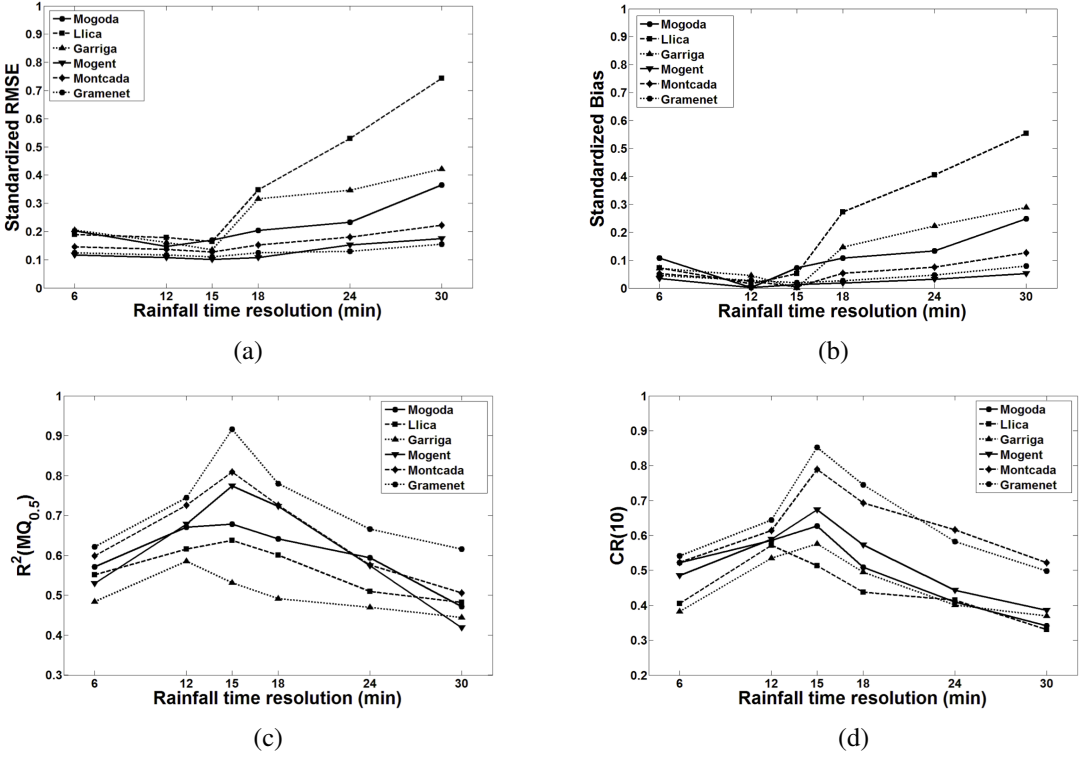

Fig. 14: Validation measures plotted versus rainfall time resolution for all stations. (a)) Root Mean Square Error (RMSE), standardized by observed peak discharge(b)) Absolute value of Bias (ME), standardized by observed peak discharge. (c)) Nash-Sutcliffe global efficiency index $R^2(MQ_{0.5})$ (d)) Containing Ratio for a confidence level of 10% $[CR(10\%)]$.

Table 1: Rainfall amount and intensity for the four study events over the entire domain of Catalonia and over the Besòs Basin.

	Max. rainfall amount (mm)		Max. rainfall intensity (mm/h)	
Data	Catalonia	Besòs	Catalonia	Besòs
2/08/2005	57.1	55.0	117.6	117.6
11–13/10/2005	348.2	81.7	129.6	108.0
13–15/11/2005	148.1	46.4	118.8	80.4
12–14/09/2006	266.1	117.6	249.6	135.6

Table 2: Validation results for the eight Z/R relationship in each of the four study cases. The numbers in the second row represent the PDF fitting method, being 1 exponential-Gamma and 2 for the Kernel smoothing density function.

Validation		August 05		October 05		November 05		September 06	
Calibration		1	2	1	2	1	2	1	2
August 05	BIAS	0.28	0.13	0.07	−0.17	0.03	−0.19	−0.09	−0.30
	Error	6.89	3.28	4.78	−21.99	17.96	−5.61	−17.90	−45.30
	RMSE	1.64	1.30	1.89	2.39	4.78	4.03	3.38	4.29
October 05	BIAS	0.33	0.32	0.02	−0.09	−0.03	−0.13	−0.12	−0.19
	Error	10.09	12.64	−1.83	−12.81	7.92	3.51	−21.30	−30.58
	RMSE	1.88	2.35	1.73	1.98	4.10	4.64	3.28	3.57
November 05	BIAS	0.21	0.19	−0.09	−0.19	−0.14	−0.23	−0.23	−0.31
	Error	4.19	4.94	−16.85	−25.12	−9.34	−12.65	−39.10	−46.58
	RMSE	1.12	1.26	2.09	2.40	3.26	3.72	3.88	4.22
September 06	BIAS	0.45	0.41	0.17	0.02	0.13	−0.02	0.02	−0.09
	Error	17.06	19.67	24.09	3.62	36.84	25.67	6.84	−11.37
	RMSE	2.84	3.52	2.28	2.04	6.43	6.64	3.33	3.34

Table 3: Comparison of results before and after of applying the advection correction.

	Best previous results			Advection results		
Index	BIAS	Error	RMSE	BIAS	Error	RMSE
Aug 05	−0.04	−1.1	1.00	0.002	−0.59	0.92
Oct 05	0.02	−1.83	1.73	0.02	−1.50	1.70
Nov 05	−0.13	3.51	3.26	−0.14	3.06	3.23
Sep 06	0.02	6.84	3.33	0.02	4.20	2.99

Table 4: Basin area (km^2), length of the main watercourse (km), slope between maximum and minimum elevation (m/m), time of concentration by the Kirpich formula (h) and requiered minimum time resoltuion of rainfall in Mediterranean regions (min) of Besòs basin stations.

	Area (km^2)	L (km)	S(m/m)	t_c (h)	Δt_{min}
Mogoda	111	31.83	0.026	3.87	12.3
Lliça	146	38.71	0.023	4.73	13.3
Garriga	151	26.41	0.026	3.36	13.5
Mogent	182	36.66	0.032	3.99	14.2
Montcada	221	43.24	0.015	6.15	15.1
Gramenet	1012	63.45	0.015	8.26	23.8

Table 5: Summary of calibration results for each parameter and all time resolutions. Table shows mean value (μ) and standard deviation (σ) of the parameter distribution.

	Parameter							
Time resolution	$\log_{10}(f)$ [mm^{-1}]		α[$-$]		K_v[$-$]		C_v [m h^{-1}]	
(min)	μ	σ	μ	σ	μ	σ	μ	σ
6	-3.05	0.92	41.6	25.8	10.1	2.82	4680	1654
12	-2.15	0.71	48.6	28.9	10.9	1.80	4643	1220
15	-2.63	0.68	53.4	27.1	11.3	2.15	4397	1313
18	-2.30	0.51	48.9	30.6	10.7	1.75	4563	1818
24	-2.32	0.29	44.0	28.8	10.1	1.95	4593	1655
30	-2.65	0.69	50.6	24.4	11.1	2.77	3415	1439

Table 6: Validation results for the eight Z/R relationship in each of the four study cases. The numbers in the second row represent the PDF fitting method, being 1 exponential-Gamma and 2 for the Kernel smoothing density function.

Validation		August 05		October 05		November 05		September 06	
Calibration		1	2	1	2	1	2	1	2
August 05	BIAS	0.28	0.13	0.07	−0.17	0.03	−0.19	−0.09	−0.30
	Error	6.89	3.28	4.78	−21.99	17.96	−5.61	−17.90	−45.30
	RMSE	1.64	1.30	1.89	2.39	4.78	4.03	3.38	4.29
October 05	BIAS	0.33	0.32	0.02	−0.09	−0.03	−0.13	−0.12	−0.19
	Error	10.09	12.64	−1.83	−12.81	7.92	3.51	−21.30	−30.58
	RMSE	1.88	2.35	1.73	1.98	4.10	4.64	3.28	3.57
November 05	BIAS	0.21	0.19	−0.09	−0.19	−0.14	−0.23	−0.23	−0.31
	Error	4.19	4.94	−16.85	−25.12	−9.34	−12.65	−39.10	−46.58
	RMSE	1.12	1.26	2.09	2.40	3.26	3.72	3.88	4.22
September 06	BIAS	0.45	0.41	0.17	0.02	0.13	−0.02	0.02	−0.09
	Error	17.06	19.67	24.09	3.62	36.84	25.67	6.84	−11.37
	RMSE	2.84	3.52	2.28	2.04	6.43	6.64	3.33	3.34

Table 7: Comparison of results before and after of applying the advection correction.

	Best previous results			Advection results		
Index	BIAS	Error	RMSE	BIAS	Error	RMSE
Aug 05	−0.04	−1.1	1.00	0.002	−0.59	0.92
Oct 05	0.02	−1.83	1.73	0.02	−1.50	1.70
Nov 05	−0.13	3.51	3.26	−0.14	3.06	3.23
Sep 06	0.02	6.84	3.33	0.02	4.20	2.99

Table 8: Validation results for the selected gauge stations.

		Time resolution					
gauge station	Measure	30 min	24 min	18 min	15 min	12 min	6 min
Lliça	RMSE	16.212	11.546	7.577	3.586	3.911	4.142
	Bias	−12.072	−8.843	−5.939	−1.143	0.325	1.568
	$R^2(\mathrm{MQ}_{0.5})$	0.315	0.333	0.392	0.416	0.387	0.360
	CR (10%)	0.254	0.319	0.337	0.365	0.440	0.312
Montcada	RMSE	24.398	19.708	16.718	13.993	14.893	16.003
	Bias	−13.842	−8.157	−5.891	0.548	2.744	5.747
	$R^2(\mathrm{MQ}_{0.5})$	0.330	0.376	0.474	0.528	0.474	0.391
	CR (10%)	0.522	0.616	0.693	0.789	0.614	0.523
Gramenet	RMSE	85.530	71.237	68.725	60.656	64.435	68.516
	Bias	−43.843	−25.817	−14.795	10.658	15.365	25.131
	$R^2(\mathrm{MQ}_{0.5})$	0.398	0.421	0.438	0.521	0.432	0.356
	CR (10%)	0.498	0.520	0.539	0.686	0.592	0.504
Garriga	RMSE	9.726	8.003	7.278	3.108	3.736	4.741
	Bias	−6.669	−5.142	−3.385	0.005	1.049	1.644
	$R^2(\mathrm{MQ}_{0.5})$	0.290	0.307	0.321	0.347	0.382	0.316
	CR (10%)	0.284	0.308	0.381	0.490	0.395	0.201
Mogent	RMSE	24.586	21.422	15.130	14.257	15.020	16.460
	Bias	−7.331	−4.393	−2.524	−1.789	0.214	4.803
	$R^2(\mathrm{MQ}_{0.5})$	0.208	0.375	0.472	0.545	0.443	0.346
	CR (10%)	0.304	0.389	0.482	0.614	0.589	0.485
Mogoda	RMSE	11.192	7.138	6.234	5.206	4.505	6.213
	Bias	7.599	4.100	3.295	2.201	−0.049	3.310
	$R^2(\mathrm{MQ}_{0.5})$	0.243	0.388	0.419	0.443	0.438	0.373
	CR (10%)	0.284	0.341	0.424	0.543	0.468	0.435